Revision 1

The diffusion behavior of hydrogen in plagioclase feldspar at 800-1000°C: Implications for re-equilibration of hydroxyl in volcanic phenocrysts

Elizabeth A. Johnson[1,2,3]

George R. Rossman[2]

1. Department of Geology and Environmental Science, James Madison University, 395 S. High St., MSC 6903, Harrisonburg, VA 22807. e-mail: johns2ea@jmu.edu

2. Division of Geological and Planetary Sciences, California Institute of Technology, MS 170-25, Pasadena, CA 91125-2500

3. Department of Earth and Space Sciences, University of California Los Angeles, Los Angeles, California 90095, USA

ABSTRACT

To be able to use structural hydroxyl (OH) concentrations preserved in volcanic phenocrysts to constrain magmatic water content prior to eruption, it is first necessary to understand the diffusive behavior of hydrogen in plagioclase. In this study, diffusion coefficients for a natural OH-bearing plagioclase feldspar ($Ab_{66}An_{31}Or_3$) were determined from a series of integrated loss heating experiments performed at 800-1000°C and 1 atm under air, nitrogen gas, and a CO_2-H_2 mixture at the FMQ oxygen buffer. Hydrogen diffusion was found to be isotropic within analytical error. Using a one-dimensional diffusive loss model for an infinite slab, the diffusion behavior for hydrogen

in plagioclase is described by the diffusion parameters log D_0 = -1.62±0.31 (m^2/s) and E_A=266±77 kJ/mol, and log D_0 = -0.97±0.35 (m^2/s) and E_A=278±90 kJ/mol for experiments only conducted under nitrogen gas. Nearly complete (83-97%) loss of OH from the andesine was achieved in 900°C and 1000°C heating series, except for the 900°C FMQ buffer experiment in which only 64% of the total OH was lost after 21.6 days of cumulative heating. The diffusion rates of hydrogen in the plagioclase after 800-1000°C are similar to interpolated diffusion rates for sodium diffusion in An_{30} feldspar, implying that Na^+ and H^+ both diffuse via Frenkel defects involving the large cation sites and interstitial ions. The diffusion coefficient (*D*) values for hydrogen in plagioclase are lower than most reported diffusion data for hydrogen in nominally anhydrous minerals, and are most similar to *D* reported for pure forsterite, unaffected by iron redox reactions. Based on the hydrogen diffusion parameters in this study, a 1 mm spherical plagioclase phenocryst experiencing dehydration under lowered water activity during ascent and eruption at 800°C retains 50% of its initial OH concentration after 34 days. At 900°C and 1000°C, a 1 mm phenocryst retains 50% of its initial OH concentration after only 1.3 days and 0.25 day, respectively. OH concentrations in plagioclase are therefore most indicative of magmatic water contents during the latest stages of ascent and eruption.

KEYWORDS: IR SPECTROSCOPY: OH in plagioclase, DIFFUSION: H in plagioclase, HIGH-TEMPERATURE STUDIES, IGNEOUS PETROLOGY.

INTRODUCTION

Essentially all anhydrous minerals, including common rock-forming minerals such as feldspars, pyroxenes, olivine, garnet, and quartz, contain minor to trace amounts of hydrogen incorporated into their structures in the form of OH, H_2O, or NH_4^+ (Solomon

and Rossman 1988; Bell and Rossman 1992; Bell 1993; Rossman 1996; Beran and Libowitzky 2006; Johnson 2006; Skogby 2006). Several studies have inferred water activity or concentration in igneous and metamorphic environments using measurements of structural OH (e.g., Bell and Rossman (1992); Ingrin and Skogby (2000); Johnson (2006). However, other factors in addition to water activity, including crystallographic constraints (Johnson and Rossman 2004), crystal chemistry (Vlassopoulos et al. 1993), oxygen fugacity (Peslier et al. 2002), and diffusive uptake or loss (Ingrin and Blanchard 2006; Farver 2010) can affect hydroxyl concentrations. Redox-driven diffusive loss of OH from olivine has been used to estimate magma ascent rate (Demouchy et al. 2006; Peslier and Luhr 2006; Peslier et al. 2008). In order to correctly interpret the geologic significance of structurally-bound hydrogen concentrations preserved in nominally anhydrous minerals, the diffusion behavior of hydrogen must be characterized in common minerals, including the feldspar group.

Two previous studies addressed hydrogen diffusion in structural H_2O-bearing alkali feldspars from pegmatites. Ordered alkali feldspars contain two types of structurally bound water molecules as defined by their infrared bands: Type I with stretching modes at 3620 cm^{-1} and 3550 cm^{-1}, and Type II with stretching modes at 3440 cm^{-1} and 3280 cm^{-1} (Aines and Rossman 1985; Hofmeister and Rossman 1985a; Johnson and Rossman 2003; Johnson and Rossman 2004). High-temperature infrared spectroscopy of microcline during step-heating experiments indicate that Type II H_2O is lost by 400°C and Type I is not fully removed until 660°C (Aines and Rossman 1985). A third type of unknown hydrous species formed irreversibly during the heating process. A diffusion mechanism was not proposed in this survey study.

Kronenberg et al. (1996) determined the diffusivity of hydrogen in the range 500-900°C in adularia ($Or_{90.2}Ab_{8.7}An_{0.0}Cs_{1.1}$) from Kristallina, Switzerland, containing about 180 ppm H_2O by weight. The diffusion coefficient *D* was determined at each experimental temperature by measuring loss of mid-infrared band absorbance of the OH stretch frequencies of H_2O. Hydrogen diffusion in H_2O-bearing adularia ($D = 2.2\times10^{-11}$ m^2/s at 900°C) is rapid compared to diffusion in many nominally anhydrous minerals (Ingrin and Blanchard 2006), although it is similar to the diffusion rate in quartz (Kronenberg et al. 1996). Feldspars were also annealed under hydrous conditions in Kronenberg et al. (1996), but quantification of water gain and loss was difficult for these experiments because of dissolution and precipitation on surfaces of slabs. Two possible hydrogen diffusion mechanisms were proposed: 1) movement of interstitial protons or 2) diffusion of mobile H_2O defects (Kronenberg et al. 1996). Mechanism 1) was deemed more likely due to the similarity of diffusion behavior between adularia and β-quartz.

In this study we determine hydrogen diffusion parameters for OH-bearing plagioclase feldspar at 800-1000°C in air, N_2, and a CO_2-H_2 mixture. A hydrogen diffusion mechanism is proposed and the diffusivity data are used to model rates of diffusive loss of hydrogen from plagioclase phenocrysts during volcanic eruptions.

METHODS

Experimental

The plagioclase feldspar used in this study, sample GRR1389/CIT13759, is a natural andesine crystal ($Ab_{66}An_{31}Or_3$) from a basaltic tuff near Halloran Springs, CA, at the western edge of the Cima volcanic field (Wise 1982; Hofmeister and Rossman 1984).

The andesine contains minor amounts of both ferric and ferrous iron (0.11 wt% Fe_2O_3 and 0.03 wt% FeO; (Hofmeister and Rossman 1984; Hofmeister and Rossman 1985b). The OH concentration of this feldspar was determined to be 510±90 ppm H_2O with ^1H MAS NMR spectroscopy, and its mid-IR and near-IR spectra were presented and described in Johnson and Rossman (2003). The total Fe concentration (0.05 mol Fe/L andesine) is three times lower than the H concentration (0.15 mol H/L andesine). The plagioclase is a very large (>2 cm), transparent, colorless crystal with a few macroscopic fractures and a few melt inclusions that only occur immediately adjacent to the rim of the crystal (Johnson and Rossman 2004). The OH concentration has an estimated variation of ±50 ppm H_2O across the crystal. This was determined from a comparison of integrated band areas per mm thickness for each of the 18 polished slabs produced from slicing the original crystal along two crystallographic directions, as reported in Appendix Table 1A.

The high quality and high OH concentration of the plagioclase makes it an ideal candidate for hydrogen diffusion studies. Polished slabs free of inclusions, ≥ 3 mm wide in the smallest dimension and ranging from 0.126 to 0.908 mm thick were prepared in two different crystallographic orientations in order to evaluate the extent of anisotropic hydrogen diffusion in the feldspar. Polished slabs were prepared either parallel to the {010} cleavage (labeled as || (010)), or parallel to the {001} cleavage (labeled as ⊥ (010)). Slab orientation was confirmed using optical interference figures. Diffusion properties were determined along the thin direction of each slab, so for a slab polished parallel to {010}, diffusion was determined along [010]*, and for a slab with polished sides parallel to {001}, diffusion was determined ⊥ ~[010]*.

Three sets of heating experiments were performed at Caltech: 1) under N_2 gas at 800°C, 900°C, and 1000°C; 2) in air at 900°C and 1000°C; and 3) under a CO_2-H_2 gas mixture at the FMQ buffer and 900°C. At least one polished slab || (010) and one slab ⊥ (010) were included in each set of heating experiments. The experiments in air were competed in a muffle furnace with a programmable temperature controller. The experiments in N_2 and CO_2-H_2 were run in a horizontal silica glass tube furnace monitored by an externally controlled thermocouple. The variation in temperature was less than 3°C across the area ~5 cm in length in the center of the furnace where the samples were placed during heating. The CO_2-H_2 gas mixture was held at 98.11 vol% CO_2, corresponding to the FMQ buffer at 900°C ($\log(fO_2) = -12.66$; Deines et al. 1974; Frost 1991). The duration of a particular heating run was timed from insertion of the ceramic boat containing the samples into the center of the tube until removal of the boat from the furnace.

Infrared spectra were obtained at the Mineral Spectroscopy Lab at Caltech using the Thermo-Nicolet Magna 860 FTIR spectrometer with 4 cm^{-1} resolution, a CaF_2 beamsplitter, MCT-A detector, and a $LiIO_3$ Glan-Foucalt prism polarizer. Spectra were averaged over 256 scans. For integrated loss measurements, polarized spectra were obtained in the main compartment of the spectrometer using a 1000 μm circular aperture in the center of the polished slab before heating and after each heating step. The baseline underneath the OH bands does not curve and is nearly flat (Figure 1). A linear baseline was fit from 3650-2650 cm^{-1} using the Thermo-Nicolet OMNIC software and removed from each spectrum before integration.

This study is concerned with changes in the OH concentration during heating rather than absolute OH concentration, so the total OH concentration at each time step (including the initial OH concentration before heating) is represented simply by the sum of the areas of the mid-IR OH absorption bands (2700-3600 cm^{-1}) in the two polarized spectra obtained on each slab. For the original unheated slabs, this is equivalent to the original OH concentration in the mineral, 510 ppm H_2O. For polished slabs ||{010}, these are the *X* and *Y'* principal optical directions in andesine. For the {001} slabs, spectra were obtained with **E**||*X* and **E**||*Z*'. The total relative error on each spectral measurement is estimated at ±5% (Johnson and Rossman 2003).

Diffusion modeling

Diffusion coefficients were calculated from integrated loss experiments using a one-dimensional model of diffusion in an infinite plane sheet with an initial uniform distribution of hydrogen, with surfaces that are kept at constant and equal concentrations. The appropriate diffusion equation for this situation is Eqn 4.18, p.48, of Crank 1975):

$$\frac{M_t}{M_\infty} = 1 - \sum_{n=0}^{\infty} \frac{8}{(2n+1)^2 \pi^2} \exp\{-D(2n+1)^2 \pi^2 t / 4L^2\} \quad (1)$$

In which M_t is the amount of diffusing substance that has left the sheet after time *t*, M_∞ is the amount of diffusing substance that has left the sheet after infinite time, 2*L* is the thickness of the sheet, and *D* is the diffusion coefficient.

In the diffusion experiments, the infinite plane sheet is approximated with a polished slab of plagioclase with a thickness much less than its width. Thus, 2*L* in Equation 1 corresponds to the thickness of the polished slab and *t* is the cumulative duration of heating at a particular temperature. The quantity M_t is determined from the

amount of OH band area lost after time t (M_t = 100 – % of the original band area at time t) because the infrared spectra measure the integrated OH concentration through the thickness of the slab. M_∞, the amount of diffusing substance that has left the sheet after infinite time, is determined by measuring the remaining OH concentration at very long heating times for each temperature and gas condition. The diffusion coefficient D is determined by a least-squares fit of Equation 1 to a series of measurements of t and M_t.

RESULTS

Representative polarized infrared spectra of the andesine OH bands obtained during the heating sequence at 1000°C under N_2 gas are shown in Figure 1. Band position and shape are the same as reported in Johnson and Rossman (2003). The band height and area decrease as the OH is lost from the crystal with progressive heating, but the band shape and position do not change, indicating that the bonding environment of the OH within the plagioclase structure does not change during the heating experiments.

Data from each heating series are plotted in Figures 2-4 and compiled in Appendix Table A1. Images of polished slabs used in this study are compiled in Appendix Figure 1A and include slabs that experienced gas failure during the last heating step. Two slabs (0.290 and 0.390 mm) from the FMQ buffer experiments at 900°C show surface pitting which occurred during the last heating step when the gas mixture was expended. The third polished slab under FMQ buffer conditions did not experience a failed run, and does not show surface pitting. Some of the polished slabs had scratches near the edges where the polishing was not perfect. These scratches seem to be affected

by heating, producing cloudiness presumably due to surface corrosion. We avoided these areas, as well as fractures, when making the FTIR measurements.

Diffusion parameters determined from least-squares fits to each dataset are summarized in Table 1. Figures 2A, 2B, and 2C are data and best fit curves from the experiments conducted under N_2 gas at 800°C, 900°C, and 1000°C, respectively. Samples heated at 900°C and 1000°C under N_2 at long times experienced almost total loss of OH from the plagioclase (M_∞ = 0.9 at 900°C and M_∞ =0.97 at 1000°C). For experiments at 800°C, it was necessary to assume a value of M_∞ due to the long heating times needed to produce significant OH loss (25 days for the longest completed experiment). M_∞ was chosen as 1 in order to minimize the least squares error of the fit to the data. If M_∞ is instead assigned a value of 0.9 as at 900°C, the value of D at 800°C increases from 2.6 x 10^{-15} m^2/s to 4.4 x 10^{-15} m^2/s

Figures 3A and 3B are data and fit curves for integrated loss experiments under air at 900°C and 1000°C. Samples heated in air at 900°C and 1000°C experienced near total loss of OH at long heating times (M_∞ is 0.86 to 1 at 900°C and M_∞ = 0.83 at 1000°C). Data obtained at 900°C at the FMQ buffer are in Figure 4. Under the CO_2-H_2 gas mixture held at FMQ buffer conditions, only 64% of the original OH was lost (M_∞ = 0.64).

Under all experimental conditions, hydrogen diffusion is isotropic. There is no observed difference in the rate of diffusive loss for polished slabs cut perpendicular to (010) compared to those cut parallel to (010) (Figures 2-4). The diffusion coefficients D calculated from the integrated loss experiments under N_2 and air (Table 1 and Figure 4)

are the same within error for the 1000°C experiments. The calculated *D* values for experiments under air and FMQ conditions are lower than *D* calculated for experiments under N_2 at 900°C.

The temperature dependence of the diffusion data is described by the Arrhenius equation:

$$D = D_0 e^{\frac{-E_A}{RT}} \quad (2)$$

where D_o is the pre-exponential factor in m^2/s, E_A is the activation energy in kJ/mol, R is the gas constant (0.008314 kJ/mol/K), and T is temperature in Kelvin. The logarithmic form of Equation 2 used in a linear least-squares fit of all *D* values determined for the An_{30} crystal in this study produced:

$\log D_0 = -1.62 \pm 0.31$ (m^2/s) and $E_A = 266 \pm 77$ kJ/mol.

In the case of experiments conducted under N_2 gas only, the least-squares fit of Equation 2 produced:

$\log D_0 = -0.97 \pm 0.35$ (m^2/s) and $E_A = 278 \pm 90$ kJ/mol.

The *D* values from this study and the fit line through all of the An_{30} data are plotted in Figure 5 and in 6A along with representative diffusion data for hydrogen in other nominally anhydrous minerals, including H_2O-bearing alkali feldspar (adularia; Kronenberg et al. 1996). Diffusion coefficients in plagioclase feldspar as reported in this study are two orders of magnitude lower than those at the same temperature for adularia feldspar. The *D* values for plagioclase are also lower than those reported for most other nominally anhydrous minerals, and are most similar to charge-coupled diffusion determined from hydrogenation experiments with pure forsterite olivine (activation

energy of 211±18 kJ/mol and anisotropic diffusion with log D_0 = -3.3 to -4.4 (m^2/s); Demouchy and Mackwell 2003).

A plot of diffusion data for other cations and oxygen in feldspars (Figure 6B) shows that the hydrogen diffusion behavior in andesine is most similar to sodium diffusion in feldspars. There are no reported sodium diffusion data for An_{30} plagioclase, but sodium isotopic tracer diffusion in An_{60} plagioclase normal to (001) has E_A = 268±11 kJ/mol and log D_0 = -3.10±0.46 (m^2/s) (Behrens et al. 1990).

Loss of OH from plagioclase phenocrysts during magma ascent and eruption is modeled using the hydrogen diffusion data from the experiments under N_2 gas. The model assumes that depressurization during ascent results in devolatization of magma and subsequent dehydration of the phenocrysts. The phenocrysts are approximated as isotropic spheres, and the diameter of the sphere represents the shortest diameter of a non-equant plagioclase phenocryst. The total amount of OH lost from the spherical plagioclase phenocrysts at each time is calculated using Equation 6.20, p.91, from Crank (1975). This equation requires a value for M_∞, the total OH lost after long times. For these calculations M_∞ is assumed to be 1 (100% loss) since this was true for the experiments conducted under N_2 gas. The total fractional loss of OH under the FMQ buffer was much less (M_∞ = 0.64), so modeled % loss values should be considered minimum values under more reducing conditions. Model results are plotted for 800°C, 900°C, and 1000°C under N_2 gas in Figure 7 for a phenocryst diameter of 1mm. At 800°C, a 1 mm plagioclase retains greater than 50% of its structural OH for more than a month (34 days). In contrast, a 1 mm plagioclase held at 900°C loses 50% of structural

OH over about 1.3 days, and only about 6 hours is needed for a 1mm plagioclase held at 1000°C to lose half of its OH content.

DISCUSSION

Hydrogen sites and hydrogen diffusion

Infrared spectroscopic data show that hydrogen is incorporated into the plagioclase structure as OH groups (Hofmeister and Rossman 1985b; Hofmeister and Rossman 1986, Johnson and Rossman 2003). The polarized infrared spectra of the OH bands have a maximum absorption parallel to the ***a*** crystallographic axis, which is the orientation produced by hydrogen bonding with O_A2 oxygen around the large cation (A) sites in the feldspar structure (Behrens and Müller 1995). The OH bands in plagioclase are broad (Figure 1), even at low temperatures (Johnson and Rossman 2003), suggesting that H^+ also bonds to other oxygen sites surrounding the A sites with a range of hydrogen bonding distances and strengths. It is not known if interstitial OH exists in feldspars.

The activation energy of 266±77 kJ/mol for An_{30} plagioclase (Figure 6A) is larger than the activation energy for hydrogen diffusion in adularia (172±15 kJ/mol). Kronenberg et al. (1996) proposed that the hydrogen diffusion in adularia occurs via migration of interstitial protons, similar to the proposed mechanism for hydrogen diffusion in β-quartz which has an activation energy of 176 kJ/mol (Kats et al. 1962). Hydrogen diffusion in plagioclase therefore does not proceed simply by interstitial hopping of H^+ ions.

Hydrogen diffusion coefficients in plagioclase are lower than hydrogen diffusion coefficients in most other nominally anhydrous minerals, but are most similar to diffusion

of hydrogen controlled by metal vacancy defects in pure forsteritic olivine (Figure 6A; Demouchy and Maxwell 2003). Diffusion experiments for Fe-bearing olivine (Mackwell and Kohlstedt 1990; Demouchy and Maxwell 2003) as well as data for other Fe-bearing nominally anhydrous minerals (Figure 6a; summarized in Ingrin and Blanchard 2006) indicate that H diffusion occurs through fast redox exchange involving interstitial H and electron holes (polarons) on Fe atoms.

Diffusion of cations in feldspars

The characteristics of sodium diffusion and diffusion of other relevant ions in feldspar are summarized here and in Figure 6b in order to compare hydrogen diffusion to diffusion behaviors of these ions.

Cation diffusion data for major and trace elements as well as Na-K and CaAl-NaSi interdiffusion are compiled in Cherniak (2010). Oxygen diffusion is strongly influenced by water fugacity (e.g. Farver and Yund 1990), and H_2O molecules are thought to be the oxygen-transporting species in the feldspar structure. The rate of Al/Si disordering in albite and microcline is increased in the presence of hydrogen gas (Goldsmith 1986, 1987, 1988). In contrast, the rate of sodium diffusion in plagioclase is not affected by water pressure or Al/Si ordering within the structure (Behrens et al. 1990). Potassium diffusion is similar under dry and hydrothermal conditions for albite, oligoclase, and labradorite (Giletti and Shanahan 1997). Calcium diffusion is not affected by changes in oxygen fugacity in An_{60-66} plagioclase (Behrens et al. 1990).

Sodium self-diffusion data (diffusion measured using isotopic tracers in the absence of a strong chemical gradient) was determined for An_{60-66} plagioclase, low albite, and alkali feldspars (Behrens et al. 1990; Figure 6b). Sodium diffusion in feldspars is

294 composition-dependent and is fastest in albite and slowest in Ca-rich plagioclase
295 (Petrovic 1972, 1974; Behrens et al. 1990; Cherniak 2010). Microstructural boundaries
296 in intermediate plagioclase do not have a significant effect on diffusion properties of
297 sodium. Pre-annealing to remove *b* antiphase boundaries in labradorite reduced diffusion
298 by a factor of 2.5 for samples heated in air, and had no effect on sodium diffusion rate
299 under a 50:50 CO/CO_2 gas mixture (Behrens et al. 1990). A comparison of
300 experimentally determined activation energies to calculated bond strengths points to
301 diffusion by sodium interstitial and large cation site vacancy pairs, or Frenkel defects
302 (Petrovic 1974; Behrens et al. 1990; Giletti 1993). This is in contrast to lithium diffusion
303 (Giletti and Shanahan 1997) which is interpreted to diffuse only through interstitial sites
304 based on its fast diffusion and low activation energy (E_A = 146±14 kJ/mol). Both
305 calcium and potassium diffusion occur more slowly than sodium diffusion, and calcium
306 and potassium diffusion are postulated to occur through cation-vacancy exchange only on
307 large cation sites (Petrovic 1974; Yund 1983).
308 An interesting relationship between iron oxidation and sodium diffusion was
309 found in experiments by Behrens et al. (1990). Both iron diffusion and sodium diffusion
310 are dependent upon oxygen fugacity. Optical spectroscopy of the andesine used as a
311 starting material for this study indicates that the majority (79%) of iron in this sample is
312 Fe^{3+} in tetrahedral sites ($Fe^{3+}{}_T$) with the remaining 21% incorporated as Fe^{2+} in large
313 cation sites (Hofmeister and Rossman 1984). Reduction or oxidation of iron in the
314 tetrahedral site will affect the formation of vacancies (*V*) in neighboring large cation sites
315 (*A*) to obtain local charge balance, as summarized in two equations modified from
316 Behrens et al. (1990):

317 $$2Fe_T^{2+} + 2Na_A^{+} + \tfrac{1}{2}O_2(g) \rightarrow 2Fe_T^{3+} + 2V_A + Na_2O(g) \quad (3)$$

318 $$2Fe_T^{3+} + 2V_A + 2NaAlSi_3O_8 \rightarrow 2Fe_T^{2+} + 2Na_A^{+} + Al_2O_3 + 6SiO_2 + \tfrac{1}{2}O_2(g) \quad (4)$$

319 From the perspective of sodium diffusion, oxidation of iron in the feldspar
320 structure will result in an increase in large cation site vacancies and loss of sodium from
321 the structure by volatilization (Equation 3). Reduction of iron (Equation 4) will result in
322 breakdown of the crystal structure (Behrens et al. 1990) and loss of large cation site
323 vacancies necessary for sodium diffusion.

324 Despite the anisotropic structures of the feldspar group minerals, sodium diffusion
325 in intermediate- to high-plagioclase (Behrens et al. 1990); An_{59-66}) and low albite (Bailey
326 1971) is isotropic within measurement error. Prior studies report Na diffusion rates that
327 are slightly faster (up to 1-2 orders of magnitude) normal to (001) or (110) than rates
328 normal to (010) (Bailey 1971; Petrovic 1972, 1974; Yund 1983), although it is thought
329 that these results were affected by fractured samples (Petrovic 1974).

330 **Hydrogen diffusion mechanism in plagioclase**

331 Based upon the results from this study, we propose that hydrogen diffusion in
332 plagioclase occurs as H^+-Na^+ interdiffusion on large cation site vacancies, via Frenkel
333 defect mechanisms. This conclusion is based on similar values for activation energies
334 and measured diffusion rates of hydrogen and sodium in plagioclase, the proposed
335 mechanism for sodium diffusion in feldspar, and the isotropic diffusion behavior of both
336 hydrogen and sodium in the feldspar structure.

337 The activation energy calculated for hydrogen diffusion in An_{30} is 266±77 kJ/mol.
338 This value is similar to Na diffusion activation energies determined under a range of
339 conditions for An_{60} and An_{66} (E_A = 255-284 kJ/mol; Behrens et al. 1990). The diffusion

rates for hydrogen in An_{30} plagioclase are consistent with expected values of sodium diffusion for An_{30} plagioclase. Experimentally determined hydrogen diffusion rates in An_{30} are faster than sodium diffusion rates in An_{60}, but are slower than sodium diffusion in albite (Figure 6b). Lithium diffusion is not shown in Figure 6b, but is approximately 3 orders of magnitude faster than hydrogen diffusion in An_{30} at 800°C and is not composition-dependent (Giletti and Shanahan 1997). The isotropic behavior of hydrogen diffusion in plagioclase is also consistent with the isotropic behavior of sodium diffusion in feldspars.

Since iron redox has an effect on sodium diffusion in labradorite (Behrens et al. 1990), we propose that sodium diffusion and hydrogen diffusion are coupled in plagioclase, it is important to consider the contribution of iron redox to hydrogen diffusion. The An_{30} plagioclase used in this study has a higher sodium content than labradorite , and a lower iron concentration (0.11 wt% Fe_2O_3 and 0.03 wt% FeO; (Hofmeister and Rossman 1985b) compared to the iron content (0.39-0.51 wt% Fe_2O_3) of the labradorite crystals used in the Behrens et al. (1990) experiments at 1200°C. The effect of iron redox on sodium diffusion in the Cima andesine is expected to be less than the relatively small effect (<5x difference) for labradorite.

The Cima andesine contains 0.15 mol H/L and only 0.05 mol Fe/L, so redox-driven processes are not expected to dominate the diffusion mechanism of hydrogen in these experiments. No iron diffusion data exists at 800-1000°C, making it difficult to evaluate the contribution of iron redox to hydrogen diffusion. It is important to note that no difference was observed within error for the hydrogen diffusion coefficients *D* determined under N_2, air, or the FMQ buffer at a specific temperature. In contrast, under

more reducing conditions (FMQ buffer at 900°C), the total OH loss at long heating times was only 64%, whereas total loss at 900°C was 90-100% under N_2 and air. The majority of the iron in the Cima andesine is Fe^{3+}, and heating in unbuffered or oxidized conditions will result in oxidation of the small amount of Fe^{2+} in the structure and an increase the large cation site vacancies in the crystal structure via the reaction in Equation 3. Sodium charge-coupled diffusion with hydrogen would then promote loss of OH from the structure. In a more reducing environment (FMQ), sodium would be retained via Equation 4 even during long heating times, because vacancy formation would be inhibited in large cation sites. This would inhibit OH loss from the plagioclase.

Hydrogen loss at long heating times

Experimental data at 1000°C under N_2 and 900°C and 1000°C experiments under air deviate slightly from the expected diffusive loss curves (Figures 2C, 3A, and 3B) at long heating times. This is determined by the shape of the diffusive loss curve and the deviation is present regardless of any reasonable value of M_∞. Under unbuffered conditions, iron redox and volatilization of sodium (Equations 3 and 4) could result in multicomponent diffusive behavior for hydrogen. The possible effects of diffusive loss of hydrogen from slab edges was also evaluated using a 1-D diffusive transect profile model (Crank 1975, Eqn 4.17, p.47). An edge-to-edge distance of 3 mm was used in the model because it was the minimum width for the polished slabs used in this study (Appendix Figure 1A). Using the *D* value at 1000°C in air for the longest heating time for that sample (1130 hr), diffusive loss of hydrogen penetrates 0.5 mm into the edge of the slab. For the longest heating time (1690 hours) at 900°C in air, diffusive loss penetrates only 0.2 mm into the edge of the slab. Since the infrared spectroscopic

386 measurements were obtained in the center of each slab with a 1 mm aperture, it is
387 unlikely that diffusive loss of hydrogen from slab edges affected the measurements of
388 OH loss.

389 The total loss of OH from the feldspar structure at long heating times is closest to
390 100% (M_∞ = 0.9 and 0.97) for experiments conducted under N_2 gas, whereas total loss at
391 long times is lower for experiments conducted in air (M_∞ = 0.83 and 0.86) and the lowest
392 for experiments conducted using the CO_2-H_2 gas mixture (M_∞ = 0.64). It is possible that
393 the partial pressure of hydrogen in the gas phase during the experiments controls the total
394 loss of hydrogen from the crystal, since this is expected to be very low in a N_2
395 environment and highest in the CO_2-H_2 gas mixture. Further experimental work to
396 measure hydrogen diffusion in feldspars under controlled redox conditions in the absence
397 of H_2 gas are needed to completely resolve these issues.

398 **Retention and resetting of OH in volcanic phenocrysts**

399 The OH concentrations in plagioclase phenocrysts have the potential to represent
400 magmatic water content if the partitioning behavior of water between plagioclase and
401 melt is known (Johnson 2005; Seaman et al. 2006; Yang 2012). The models presented in
402 this study assume dehydration of a phenocryst during ascent and eruption and constrain
403 the characteristic timescales of diffusive re-equilibration of OH at magmatic temperatures
404 for a 1 mm phenocryst. Explosive eruptions involving rapid magma ascent (>66 m/h)
405 from a magma chamber such as the May, 1980, Mount St. Helens eruption (e.g.
406 Rutherford and Hill 1993) are the most likely to retain plagioclase OH concentrations
407 equilibrated at depth. The rate of hydrogen diffusion at magmatic temperatures is fast
408 enough that the previous magmatic history prior to a few days before eruption, including

409 phenocryst inheritance and magma mixing within a magma chamber (Ruprecht and
410 Cooper 2012), will be erased from the plagioclase OH record due to re-equilibration.
411 Other eruptions involve slow ascent from the magma chamber to the surface. Stalling
412 during ascent can result in either degassing from or fluid fluxing of the magma in an
413 intermediate storage area (Berlo et al. 2004; Kent et al. 2007). Plagioclase crystal growth
414 also occurs during decompression (Cashman 1992). Depending on the timescales of
415 these processes, plagioclase OH can be totally or partially reset during ascent to the
416 surface. In either case of rapid or slow ascent, the OH concentrations in plagioclase are
417 expected to reflect fluid conditions in the last location where the magma spent more than
418 a few hours before eruption.
419 Recent studies (Costa et al. 2003; Berlo et al. 2004; Costa et al. 2008; Kent et al.
420 2007; Ruprecht and Cooper 2012) have used Li and Mg diffusion in plagioclase to help
421 understand the dynamics and timescales of magma ascent. Since the hydrogen diffusion
422 rate in plagioclase at magmatic temperatures is intermediate between Mg diffusion
423 (LaTourette and Wasserburg 1998) and very rapid Li diffusion (Giletti and Shanahan
424 1997), OH measurements in transects across plagioclase phenocrysts should aid our
425 understanding of eruption dynamics. As for Mg diffusion, the implied dependence of H
426 diffusion (which is similar to Na diffusion) on major element composition should be
427 taken into account for the best determination of re-equilibration times (Costa et al. 2003).
428 At least one study has found OH concentration gradients in natural volcanic plagioclase
429 and has used OH in plagioclase to infer a polybaric degassing history of Izu-Oshima
430 volcano (Hamada et al. 2011). Constraints from this study on the hydrogen diffusion
431 behavior in plagioclase, combined with measurements of OH in plagioclase and water in

melt inclusions, hold the potential to be used as a speedometer for magma transport and eruption.

Concluding remarks

Based on the results from our integrated loss experiments, diffusion of hydrogen in plagioclase (An_{30}) is slower than in H_2O-bearing alkali feldspar (Kronenberg et al. 1996). The activation energy of hydrogen diffusion in plagioclase is higher than the activation energy of hydrogen in adularia, implying that hydrogen diffusion in plagioclase does not occur through simple migration of interstitial protons as in adularia or β-quartz.

Hydrogen diffusion in plagioclase occurs via a mechanism similar to sodium diffusion: coupled interstitial and large cation site vacancy pairs, or Frenkel defects. Hydrogen diffusion in andesine matches the interpolated sodium self-diffusion rate for An_{30} feldspar. Sodium diffusion and hydrogen diffusion in plagioclase have similar activation energies, and the activation energies are not large enough to involve rearrangement of the aluminosilicate structure. Hydrogen diffusion and sodium diffusion are both isotropic in plagioclase. Although iron reduction in the tetrahedral site influences sodium self-diffusion in labradorite (Behrens et al. 1990), it is predicted to have less of an effect on sodium diffusion in the lower-Fe Cima andesine. Reduction of Fe^{3+} to Fe^{2+} may decrease the total sodium and hydrogen loss (M_∞) from plagioclase at long heating times by inhibiting formation of large cation site vacancies, as indicated by the incomplete (64%) loss of OH from the Cima andesine under FMQ conditions.

Models of diffusive loss of hydrogen from spherical plagioclase phenocrysts during magma ascent and devolatization indicate that OH concentrations in plagioclase

phenocrysts are likely to at least partially re-equilibrate during magma ascent. The OH concentrations in plagioclase phenocrysts record water activity from the last storage location in a volcanic system.

ACKNOWLEDGMENTS

This work was supported by NSF grants EAR-0409883 (EAJ) and EAR-0125767 (GRR). The authors thank S. Demouchy and D. Cherniak for their helpful reviews.

REFERENCES

Aines, R.D. and Rossman, G.R. (1985) The high temperature behavior of trace hydrous components in silicate minerals. American Mineralogist, 70, 1169-1179.

Bailey, A. (1971). Comparison of low-temperature with high-temperature diffusion of sodium in albite. Geochimica et Cosmochimica Acta, 35, 1073-1081.

Behrens, H. and Mueller, G. (1995) An infrared spectroscopic study of hydrogen feldspar ($HAlSi_3O_8$). Mineralogical Magazine, 59, 15-24.

Behrens, H., Johannes, W., and Schmalzried, H. (1990) On the mechanisms of cation diffusion processes in ternary feldspars. Physics and Chemistry of Minerals, 17, 62-78.

Bell, D.R. (1993) Hydroxyl in mantle minerals. Ph.D. thesis, California Institute of Technology, Pasadena, CA, United States.

Bell, D.R. and Rossman, G.R. (1992) Water in Earth's mantle; the role of nominally anhydrous minerals. Science, 255, 1391-1397.

Beran, A. and Libowitzky, E. (2006) Water in natural mantle minerals II: olivine, garnet, and accessory minerals. In H. Keppler and J.R. Smyth, Eds. Water in Nominally Anhydrous Minerals, 62, 169-192, Reviews in Mineralogy and Geochemistry, Mineralogical Society of America, Chantilly, Virginia.

Berlo, K., Blundy, J., Turner, S., Cashman, K., Hawkesworth, C., and Black, S. (2004) Geochemical precursors to volcanic activity at Mount St. Helens, USA. Science, 306, 1167-1169.

Blanchard, M. and Ingrin, J. (2004) Hydrogen diffusion in Dora Maira pyrope. Physics and Chemistry of Minerals, 31, 593-605.

Cashman, K.V. (1992) Groundmass crystallization of Mount St. Helens dacite, 1980-1986; a tool for interpreting shallow magmatic processes. Contributions to Mineralogy and Petrology, 109, 431-449.

Cherniak, D.J. (2010) Cation diffusion in feldspars. In Y. Zhang and D.J. Cherniak Eds. Diffusion in Minerals and Melts, 72, 691-733, Reviews in Mineralogy and Geochemistry, Mineralogical Society of America, Chantilly, Virginia.

Costa, F., Chakraborty, S., and Dohmen, R. (2003) Diffusion coupling between trace and major elements and a model for calculation of magma residence times using plagioclase. Geochimica et Cosmochimica Acta, 67, 2189-2200.

Costa, F., Dohmen, R., and Chakraborty, S. (2008) Time scales of magmatic processes from modeling the zoning patterns of crystals. Reviews in Mineralogy and Geochemistry, 69, 545-594.

Crank, J. (1975) The Mathematics of Diffusion, 2nd edition. London: Oxford University Press.

Deines, P., Nafziger, R.H., Ulmer, G.C., and Woermann, E. (1974) Temperature-oxygen fugacity tables for selected gas mixtures in the system C-H-O at one atmosphere total pressure. Bulletin of the Earth and Mineral Sciences Experiment Station, 88. The Pennsylvania State University, University Park, Pennsylvania.

Demouchy, S. and Mackwell, S.J. (2003) Water diffusion in synthetic iron-free forsterite. Physics and Chemistry of Minerals, 30, 486-494.

Demouchy, S. and Mackwell, S. (2006) Mechanisms of hydrogen incorporation and diffusion in iron-bearing olivine. Physics and Chemistry of Minerals, 33, 347-355.

Demouchy, S., Jacobsen, S.D, Gaillard, F., and Stern, C.R. (2006) Rapid magma ascent recorded by water diffusion profiles in mantle olivine. Geology, 34, 429-432.

Farver, J.R. (2010) Oxygen and hydrogen diffusion in minerals. In Y. Zhang and D.J. Cherniak Eds. Diffusion in Minerals and Melts, 72, 447-508, Reviews in Mineralogy and Geochemistry, Mineralogical Society of America, Chantilly, Virginia.

Farver, J.R. and Yund, R.A. (1990) The effect of hydrogen, oxygen, and water fugacity on oxygen diffusion in alkali feldspar. Geochimica et Cosmochimica Acta, 54, 2953-2964.

Foland, K.A. (1974) Alkali diffusion in orthoclase. In A.W. Hofmann, B.J. Giletti, H.S. Yoder Jr., and R.A. Yund, Eds. Geochemical Transport and Kinetics, 634, 77-98, Carnegie Institution of Washington Publication.

Frost, B.R. (1991) Introduction to oxygen fugacity and its petrologic importance. In D.H. Lindsley Ed. Oxide Minerals: Petrologic and Magnetic Significance, 24, 1-10, Reviews in Mineralogy and Geochemistry, Mineralogical Society of America, Chantilly, Virginia.

Giletti, B.J. (1993) Systematic behavior of cation diffusion kinetics in plagioclase. Eos Transactions, American Geophysical Union, 74 (43) Suppl., 611.

Giletti, B.J. and Shanahan, T.M. (1997) Alkali diffusion in plagioclase feldspar. Chemical Geology, 139, 3-20.

Giletti, B.J., Semet, M.P., and Yund, R.A. (1978) Studies in diffusion-- III. Oxygen in feldspars: an ion microprobe determination. Geochimica et Cosmochimica Acta, 42, 45-57.

Goldsmith, J.R. (1986) The role of hydrogen in promoting Al-Si interdiffusion in albite ($NaAlSi_3O_8$) at high pressures. Earth and Planetary Science Letters, 80, 135-138.

Goldsmith, J.R. (1987) Al/Si interdiffusion in albite: effect of pressure and the role of hydrogen. Contributions to Mineralogy and Petrology, 95, 311-321.

Goldsmith, J.R. (1988) Enhanced Al/Si diffusion in $KAlSi_3O_8$ at high pressures: the effect of hydrogen. Journal of Geology, 96, 109-124.

Hamada, M., Kawamoto, T., Takahashi, E., and Fujii, T. (2011) Polybaric degassing of island arc low-K tholeiitic basalt magma recorded by OH concentrations in Ca-rich plagioclase. Earth and Planetary Science Letters, 308, 259-266.

Hercule, S. and Ingrin, J. (1999) Hydrogen in diopside; diffusion, kinetics of extraction-incorporation, and solubility. American Mineralogist, 84, 1577-1587.

Hofmeister, A.M. and Rossman, G.R. (1984) Determination of Fe^{3+} and Fe^{2+} concentrations in feldspar by optical absorption. Physics and Chemistry of Minerals, 11, 213-224.

Hofmeister, A.M. and Rossman, G.R. (1985a) A spectroscopic study of irradiation coloring of amazonite: structurally hydrous, Pb-bearing feldspar. American Mineralogist, 70, 794-804.

Hofmeister, A.M. and Rossman, G.R. (1985b) A model for the irradiative coloration of smoky feldspar and the inhibiting influence of water. Physics and Chemistry of Minerals, 12, 324-332.

Hofmeister, A.M. and Rossman, G.R. (1986) A spectroscopic study of blue radiation coloring in plagioclase. American Mineralogist, 71, 95-98.

Ingrin, J. and Blanchard, M. (2006) Diffusion of hydrogen in minerals. In H. Keppler and J.R. Smyth, Eds. Water in Nominally Anhydrous Minerals, 62, 291-320, Reviews in Mineralogy and Geochemistry, Mineralogical Society of America, Chantilly, Virginia.

Ingrin, J. and Skogby, H. (2000) Hydrogen in nominally anhydrous upper-mantle minerals: concentration levels and implications. European Journal of Mineralogy, 12, 543-570.

Johnson, E.A. (2005) Magmatic water contents recorded by hydroxyl concentrations in plagioclase phenocrysts from Mount St. Helens, 1980-1981. Geochimica et Cosmochimica Acta, 69(10s), A743.

Johnson, E.A. (2006) Water in nominally anhydrous crustal minerals: speciation, concentration, and geologic significance. In H. Keppler and J.R. Smyth, Eds. Water in Nominally Anhydrous Minerals, 62, 117-154, Reviews in Mineralogy and Geochemistry, Mineralogical Society of America, Chantilly, Virginia.

Johnson, E.A. and Rossman, G.R. (2003) The concentration and speciation of hydrogen in feldspars using FTIR and ^{1}H MAS NMR spectroscopy. American Mineralogist, 88, 901-911.

Johnson, E.A. and Rossman, G.R. (2004) A survey of hydrous species and concentrations in igneous feldspars. American Mineralogist, 89, 586-599.

Kasper, R.B. (1975) Cation and oxygen diffusion in albite. Ph.D. dissertation, Brown University.

Kats, A., Haven, Y., and Stevels, J.M. (1962) Hydroxyl groups in β-quartz. Physics and Chemistry of Glasses, 3, 69-75.

Kent, A.J.R., Blundy, J., Cashman, K.V., Cooper, K.M., Donnelly, C., Pallister, J.S., Reagan, M., Rowe, M.C., and Thornber, C.R. (2007) Vapor transfer prior to the October 2004 eruption of Mount St. Helens, Washington. Geology, 35, 231-234.

Kronenberg, A.K., Yund, R.A., and Rossman, G.R. (1996) Stationary and mobile hydrogen defects in potassium feldspar. Geochimica et Cosmochimica Acta, 60, 4075-4094.

LaTourette, T. and Wasserburg, G.J. (1998) Mg diffusion in anorthite: implications for the formation of early solar system planetesimals. Earth and Planetary Science Letters, 158, 91-108.

Mackwell, S.J. and Kohlstedt, D.L. (1990) Diffusion of hydrogen in olivine: implications for water in the mantle. Journal of Geophysical Research, 95, 5079-5088.

583 Muehlenbachs, K. and Kushiro, I. (1974) Oxygen isotope exchange and equilibrium of
584 silicates with CO_2 or O_2. Year Book - Carnegie Institution of Washington, 73, 232-236.
585 Peslier, A.H., Luhr, J., and Post, J.E. (2002) Low water contents in pyroxenes from
586 spinel-peridotites of the oxidized, sub-arc mantle wedge. Earth and Planetary Science
587 Letters, 201, 69-86.
588 Peslier, A.H. and Luhr, J.F. (2006) Hydrogen loss from olivines from mantle xenoliths
589 from Simcoe (WA, USA) and Mexico: mafic alkalic magma ascent rates and water
590 budget of the sub-continental lithosphere. Earth and Planetary Science Letters, 242, 302-
591 319.
592 Peslier, A.H., Woodland, A.B., and Wolff, J.A. (2008) Fast kimberlite ascent rates
593 estimated from hydrogen diffusion profiles in xenolithic mantle olivines from southern
594 Africa. Geochimica et Cosmochimica Acta, 72, 2711-2722.
595 Petrovic, R. (1972) Alkali ion diffusion in alkali feldspars. Ph.D. thesis, Yale University,
596 New Haven, Connecticut.
597 Petrovic, R. (1974) Diffusion of alkali ions in alkali feldspars. In W.S. MacKenzie and J.
598 Zussman Eds. The Feldspars, Proceedings of a NATO Advanced Study Institute, 174-
599 182.
600 Rossman, G.R. (1996) Studies of OH in nominally anhydrous minerals. Physics and
601 Chemistry of Minerals, 23, 299-304.
602 Ruprecht, P. and Cooper, K.M. (2012) Integrating the uranium-series and elemental
603 diffusion geochronometers in mixed magmas fromVolcan Quizapu, Central Chile.
604 Journal of Petrology, 53, 841-871.
605 Rutherford, M.J. and Hill, P.M. (1993) Magma ascent rates from amphibole breakdown:
606 An experimental study applied to the 1980-1986 Mount St. Helens eruption. Journal of
607 Geophysical Research, 98, 19,667-19,685.
608 Seaman, S.J., Dyar. M.D., Marinkovic, N., and Dunbar, N.W. (2006) An FTIR study of
609 hydrogen in anorthoclase and associated melt inclusions. American Mineralogist, 91, 12-
610 20.
611 Skogby, H. (2006) Water in natural mantle minerals I: pyroxenes. In H. Keppler and J.R.
612 Smyth, Eds. Water in Nominally Anhydrous Minerals, 62, 155-168, Reviews in
613 Mineralogy and Geochemistry, Mineralogical Society of America, Chantilly, Virginia.
614 Solomon, G.C. and Rossman, G.R. (1988) NH_4^+ in pegmatitic feldspars from the
615 southern Black Hills, South Dakota. American Mineralogist, 73, 818-821.
616 Vlassopoulos, D., Rossman, G.R., and Haggerty, S.E. (1993) Coupled substitition of H
617 and minor elements in rutile and the implications of high OH contents in Nb- and Cr-rich
618 rutile from the upper mantle. American Mineralogist, 78, 1181-1191.
619 Wise, W.S. (1982) New occurrence of faujasite in southeastern California. American
620 Mineralogist, 67, 794-798.
621 Woods, S.C., Mackwell, S., and Dyar, D. (2000) Hydrogen in diopside: diffusion
622 profiles. American Mineralogist, 85, 480-487.
623 Yang, X. (2012) An experimental study of H solubility in feldspars: effect of
624 composition, oxygen fugacity, temperature and pressure and implications for crustal
625 processes. Geochimica et Cosmochimica Acta, 97, 46-57.
626 Yund, R.A. (1983) Diffusion in feldspars. In P.H. Ribbe Ed. Feldspar Mineralogy, 2,
627 203-222, Mineralogical Society of America, Washington, D.C.

628 Yund, R.A. and Anderson, T.F. (1978) The effect of fluid pressure on oxygen isotope
629 exchange between feldspar and water. Geochimica et Cosmochimica Acta, 42, 235-239.
630 Zhang, Y., Stolper, E.M., and Wasserburg, G.J. (1991) Diffusion of a multi-species
631 component and its role in oxygen and water transport in silicates. Earth and Planetary
632 Science Letters, 103, 228-240.
633
634

635

Figure 1. Mid-IR OH absorption bands in the *X* polarization direction on the polished slab parallel to (010) before and during progressive heating at 1000°C in N_2. Band shape and position is preserved during heating.

Figure 2. Diffusion data for experiments in N_2 gas at a) 800°C, b) 900°C, and c) 1000°C. 2L = thickness of polished slab, M_t = the fraction of OH lost at time *t*, and M_∞ = the fraction of total OH loss at very long heating times. The diffusion coefficient *D* was determined using Equation 1 (Crank 1975; solid curves).

Figure 3. Diffusion data for experiments in air at a) 900°C and b) 1000°C. 2L = thickness of polished slab, M_t = the fraction of OH lost at time *t*, and M_∞ = the fraction of total OH loss at very long heating times. The diffusion coefficient *D* was determined using Equation 1 (Crank 1975; solid curves). The dashed curve in Figure 3b is the best fit to all data at these conditions; the solid curve is the best fit to data with $M_t/M_\infty < 0.5$.

Figure 4. Diffusion data for experiments at 900°C in a CO_2-H_2 gas mixture held at the FMQ buffer. 2L = thickness of polished slab, M_t = the fraction of OH lost at time *t*, and M_∞ = the fraction of total OH loss at very long heating times. The diffusion coefficient *D* was determined using Equation 1 (Crank 1975; solid curves).

Figure 5. Arrhenius plot of hydrogen diffusion data for andesine (An_{30}) from this study. Best fit lines are for the nitrogen data only (dashed line) and for all of the data (solid line).

Figure 6. a) Diffusion data for hydrogen in nominally anhydrous silicate minerals, including hydrogen diffusion data for andesine (An_{30}) from this study. References to other data include those compiled in Ingrin and Blanchard (2006) and are: K 1962 = Kats et al. (1962); M 1990 = Mackwell and Kohlstedt (1990); Z 1991 = Zhang et al. (1991); K 1996 = Kronenberg et al. (1996); H 1999 = Hercule and Ingrin (1999); W 2000 = Woods et al. (2000); D 2003 = Demouchy and Mackwell (2003); and B 2004 = Blanchard and Ingrin (2004). b) A comparison of H diffusion to Na, K, Fe, Ca, and O diffusion in feldspars. The hydrogen diffusion data for andesine (An_{30}) is from this study. References to other data include those compiled in Cherniak (2010) and are: B 1971 = Bailey (1971); P 1972 = Petrovic (1972); F 1974 = Foland (1974); M 1974 = Muehlenbachs and Kushiro (1974); K 1975 = Kasper (1975); G 1978 = Giletti et al. (1978); B 1990 = Behrens et al. (1990); G 1997 = Giletti and Shanahan (1997); and L 1998 = LaTourette and Wasserburg (1998).

Figure 7. Percentage of initial OH concentration remaining in a spherical feldspar grain with diameter 1 mm as a function of time at 800°C, 900°C, and 1000°C using Equation 6.20, p.91 of Crank (1975) for diffusion in a solid sphere. *D* values in the models are from the experiments under nitrogen gas in this study, and under the assumption that all OH can be lost from the feldspar ($M_\infty = 1$).

Table 1. Diffusion parameters determined from integrated loss data.

Experimental conditions	Temperature (°C)	D (m^2/s)	M_∞ (Total fractional loss of H)
nitrogen gas	800	$2.6 \pm 0.8 \times 10^{-15}$	~1
air	900	$2.6 \pm 0.9 \times 10^{-14}$	0.86
air	900	$1.7 \pm 0.5 \times 10^{-14}$	1
FMQ buffer	900	$2.3 \pm 0.6 \times 10^{-14}$	0.64
nitrogen gas	900	$7.2 \pm 1.8 \times 10^{-14}$	0.9
air (fit to all data)	1000	$1.6 \pm 0.6 \times 10^{-13}$	0.83
air (fit to M_t/M_∞ <0.5)	1000	$2.3 \pm 0.8 \times 10^{-13}$	0.83
nitrogen gas	1000	$3.5 \pm 1.2 \times 10^{-13}$	0.97

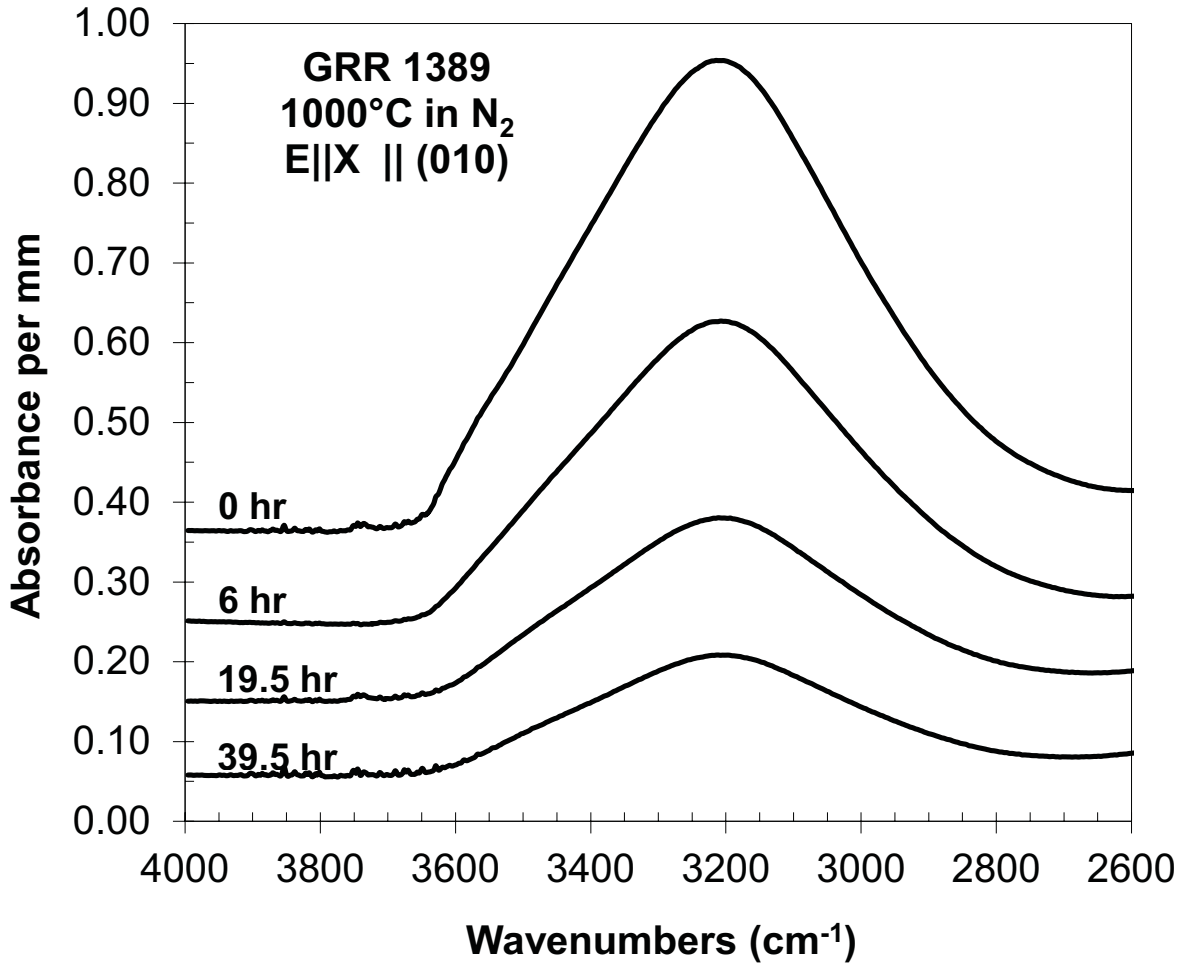
GRR 1389
1000°C in N2
E||X || (010)
0 hr
6 hr
19.5 hr
39.5 hr
Absorbance per mm
Wavenumbers (cm-1)
1.00
0.90
0.80
0.70
0.60
0.50
0.40
0.30
0.20
0.10
0.00
4000
3800
3600
3400
3200
3000
2800
2600

Figure 1

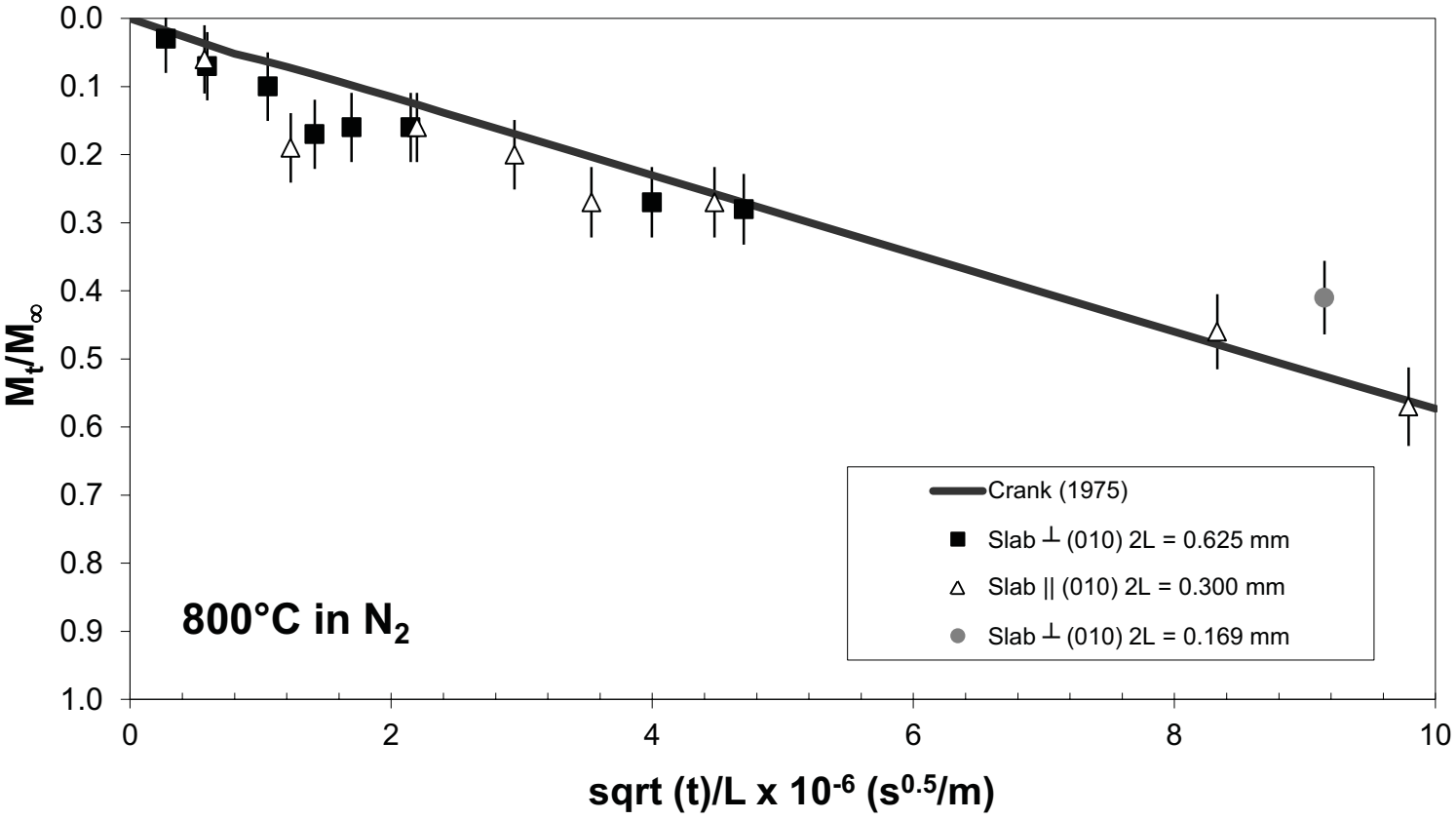
0.0
0.1
0.2
0.3
0.4
0.5
0.6
0.7
0.8
0.9
1.0
M_t/M_∞
0
2
4
6
8
10
sqrt (t)/L x 10^{-6} ($s^{0.5}$/m)
800°C in N_2
Crank (1975)
Slab ⊥ (010) 2L = 0.625 mm
Slab || (010) 2L = 0.300 mm
Slab ⊥ (010) 2L = 0.169 mm

Figure 2A

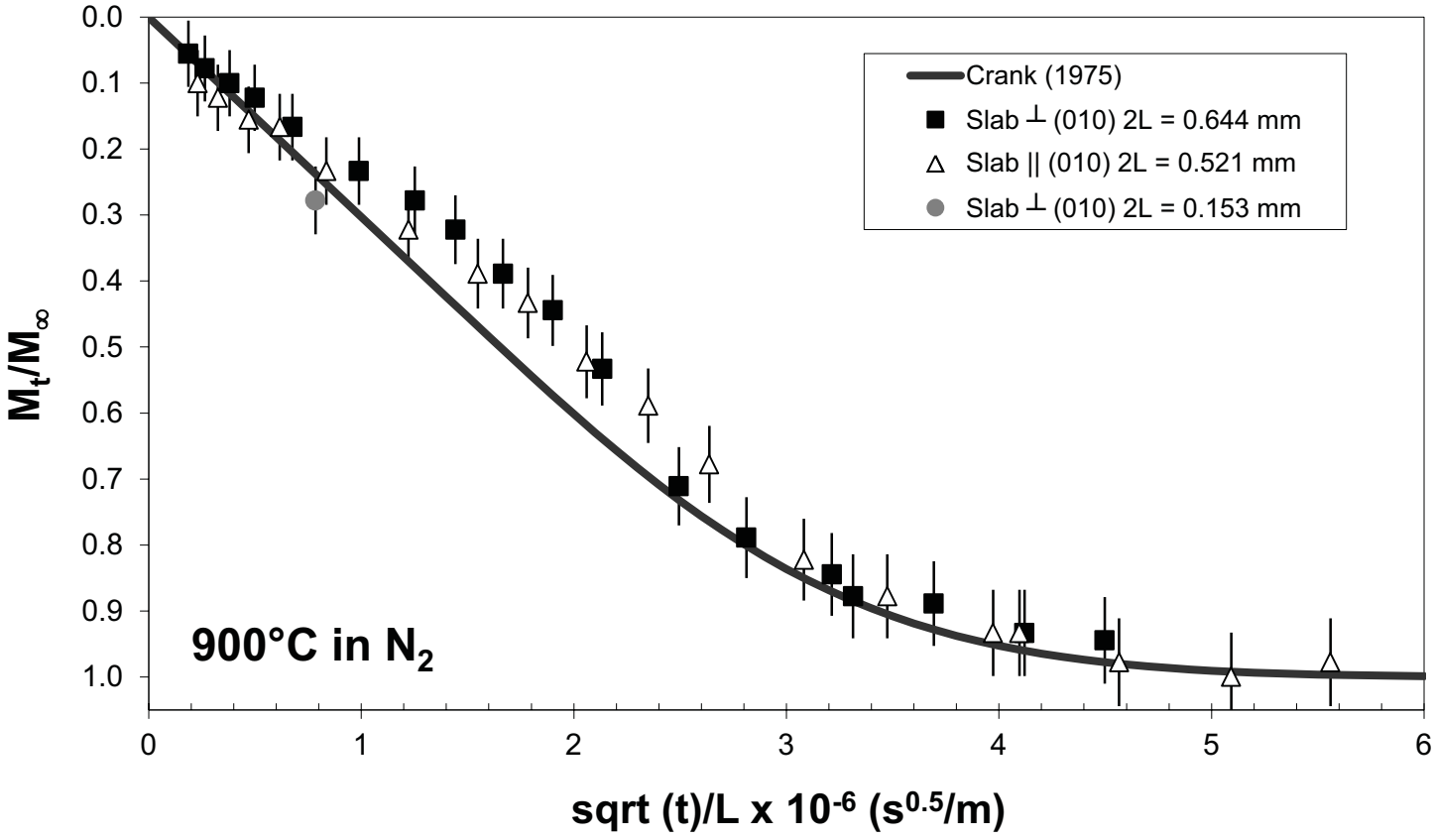
0.0
0.1
0.2
0.3
0.4
0.5
0.6
0.7
0.8
0.9
1.0
M_t/M_∞
Crank (1975)
Slab ⊥ (010) 2L = 0.644 mm
Slab || (010) 2L = 0.521 mm
Slab ⊥ (010) 2L = 0.153 mm
900°C in N_2
0
1
2
3
4
5
6
sqrt (t)/L x 10^{-6} ($s^{0.5}$/m)

Figure 2B

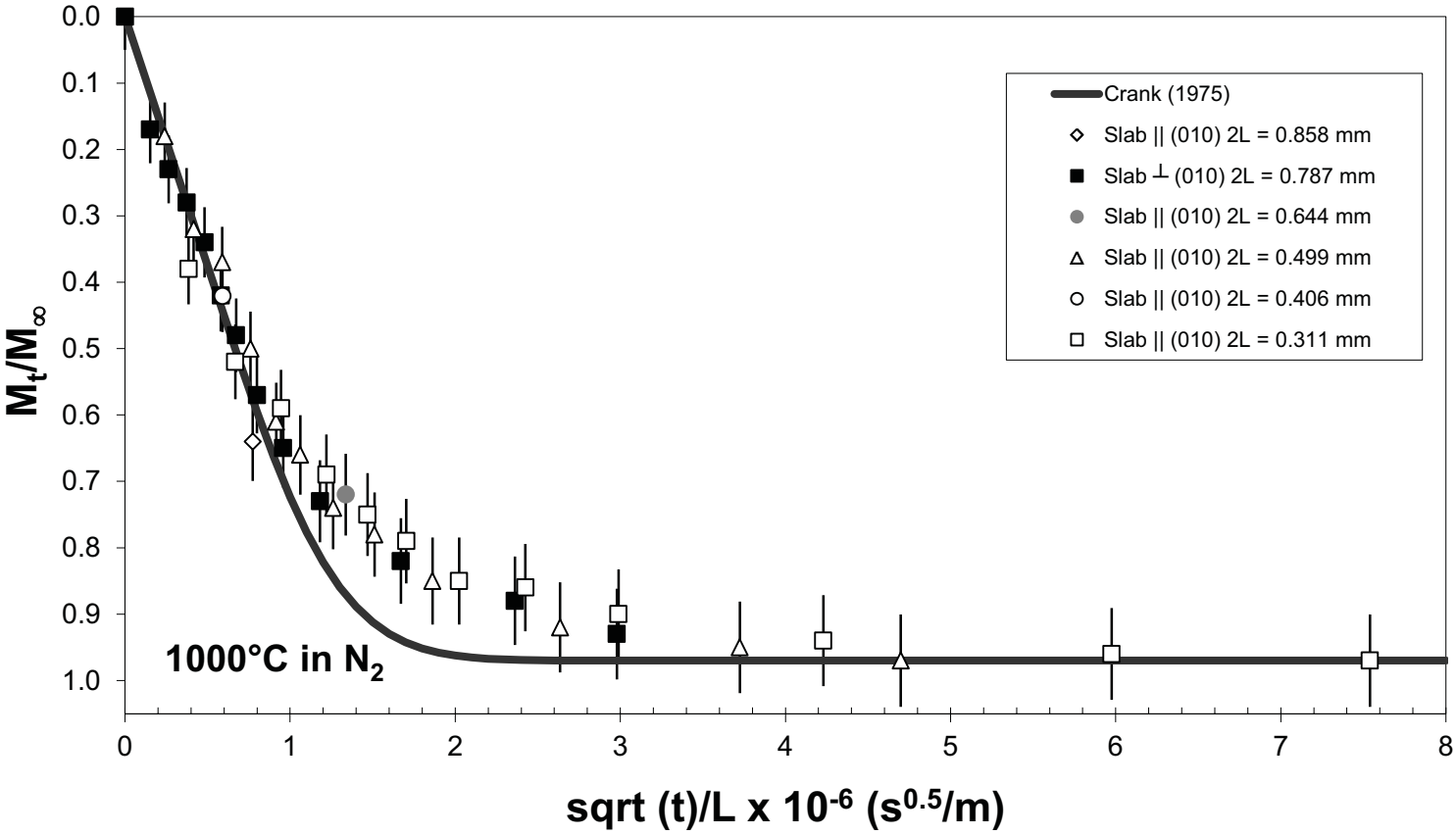
0.0
0.1
0.2
0.3
0.4
0.5
0.6
0.7
0.8
0.9
1.0
M_t/M_∞
Crank (1975)
Slab || (010) 2L = 0.858 mm
Slab ⊥ (010) 2L = 0.787 mm
Slab || (010) 2L = 0.644 mm
Slab || (010) 2L = 0.499 mm
Slab || (010) 2L = 0.406 mm
Slab || (010) 2L = 0.311 mm
1000°C in N_2
0
1
2
3
4
5
6
7
8
sqrt (t)/L x 10^{-6} ($s^{0.5}$/m)

Figure 2C

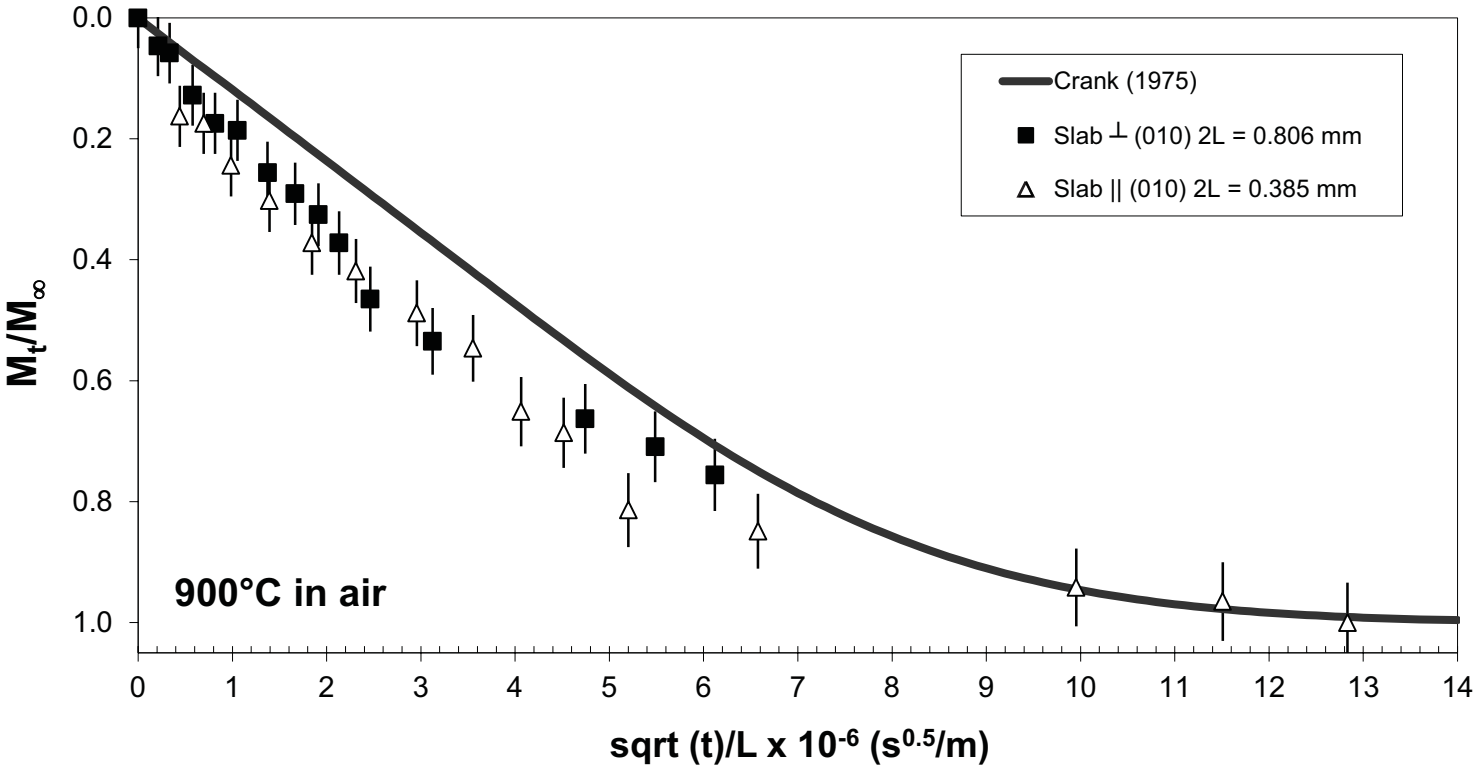
Crank (1975)
Slab ⊥ (010) 2L = 0.806 mm
Slab || (010) 2L = 0.385 mm
900°C in air
M_t/M_∞
sqrt (t)/L x 10^-6 (s^0.5/m)
0.0
0.2
0.4
0.6
0.8
1.0
0
1
2
3
4
5
6
7
8
9
10
11
12
13
14

Figure 3A

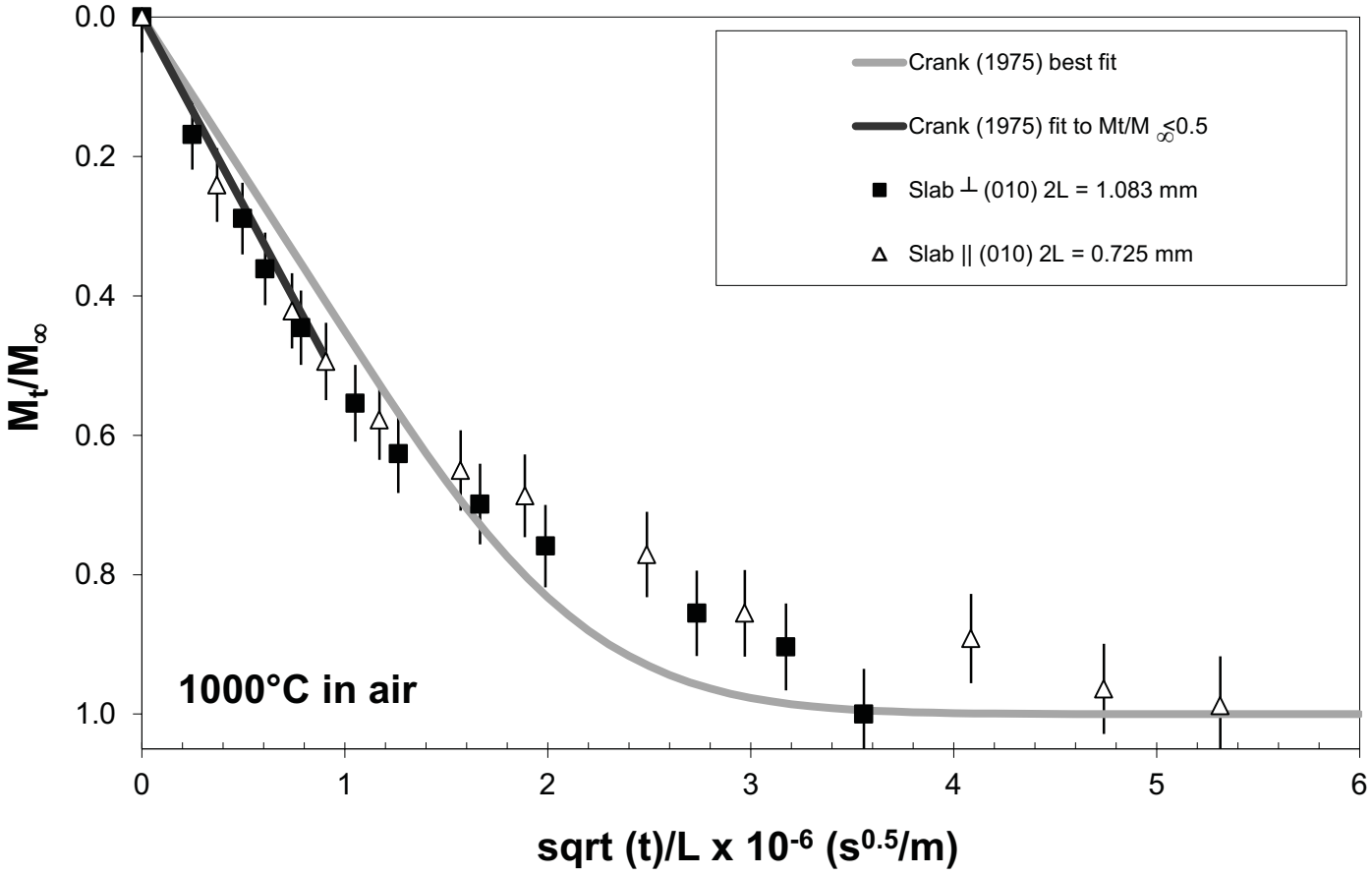
Crank (1975) best fit
Crank (1975) fit to Mt/M ∞≤0.5
Slab ⊥ (010) 2L = 1.083 mm
Slab || (010) 2L = 0.725 mm
1000°C in air
Mt/M∞
sqrt (t)/L x 10-6 (s0.5/m)
0.0
0.2
0.4
0.6
0.8
1.0
0
1
2
3
4
5
6

Figure 3B

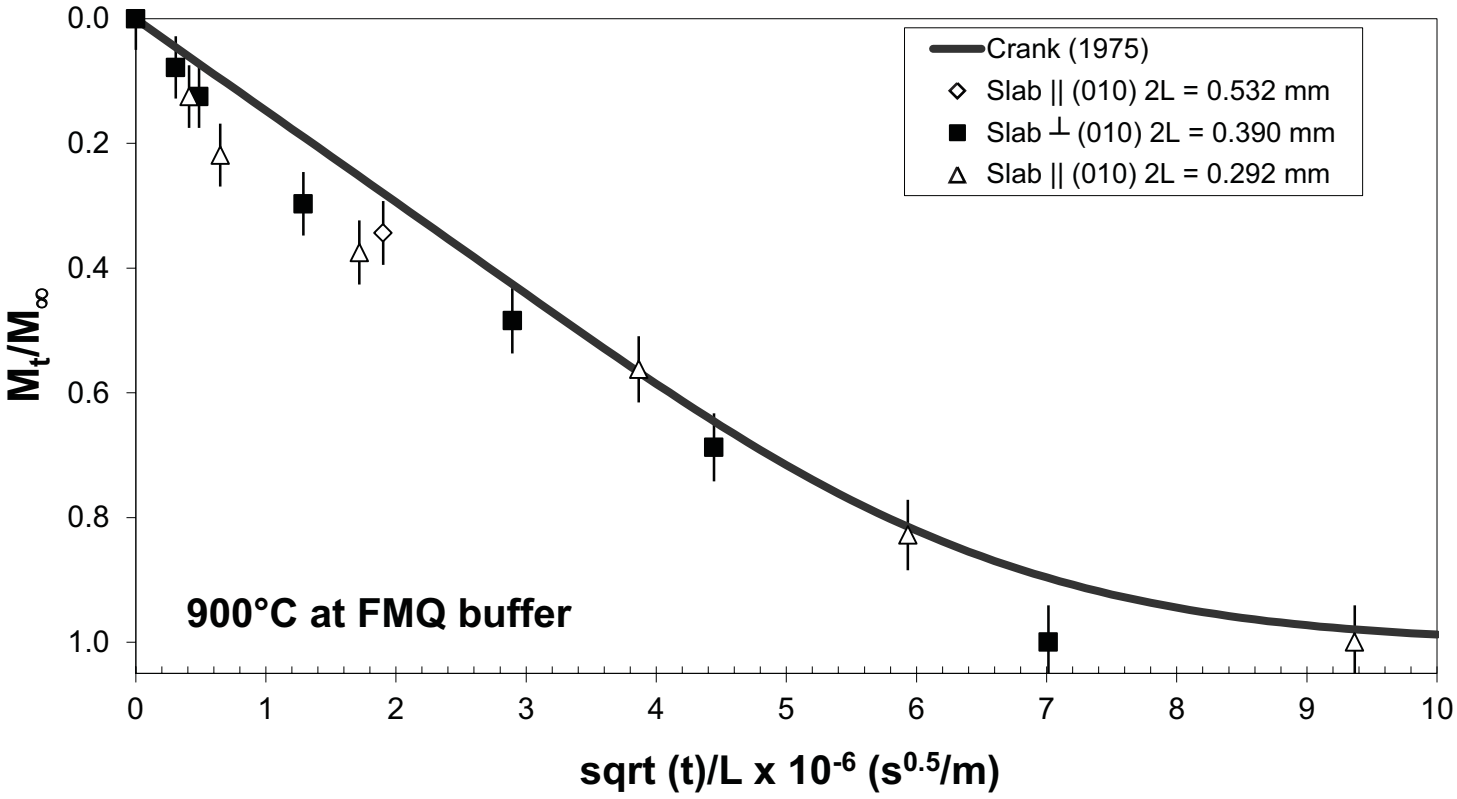
Crank (1975)
Slab || (010) 2L = 0.532 mm
Slab ⊥ (010) 2L = 0.390 mm
Slab || (010) 2L = 0.292 mm
900°C at FMQ buffer
M_t/M_∞
sqrt (t)/L x 10^{-6} ($s^{0.5}$/m)
0.0
0.2
0.4
0.6
0.8
1.0
0
1
2
3
4
5
6
7
8
9
10

Figure 4

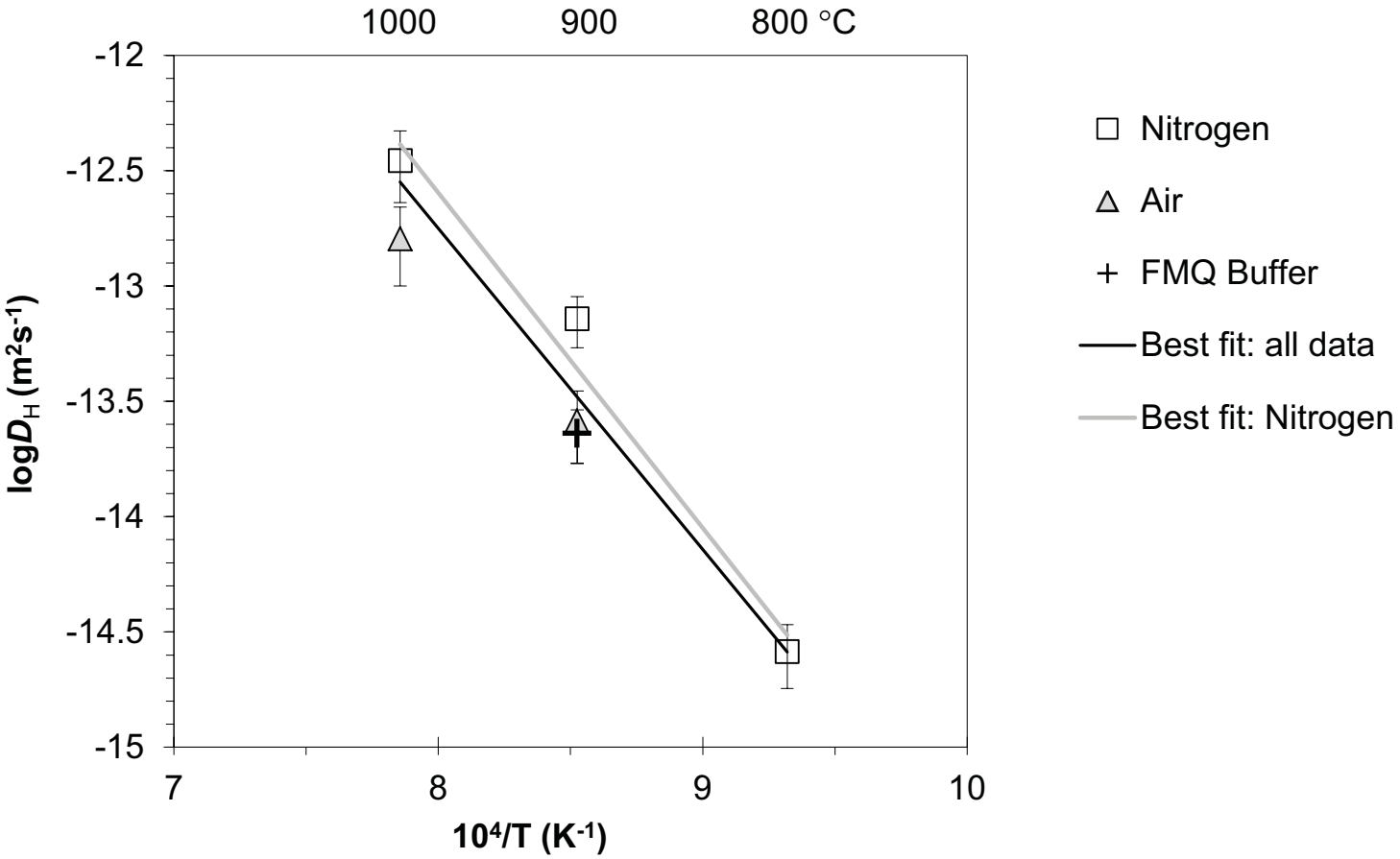
1000
900
800 °C
-12
-12.5
-13
-13.5
-14
-14.5
-15
7
8
9
10
$\log D_H$ (m^2s^{-1})
$10^4/T$ (K^{-1})
Nitrogen
Air
FMQ Buffer
Best fit: all data
Best fit: Nitrogen

Figure 5

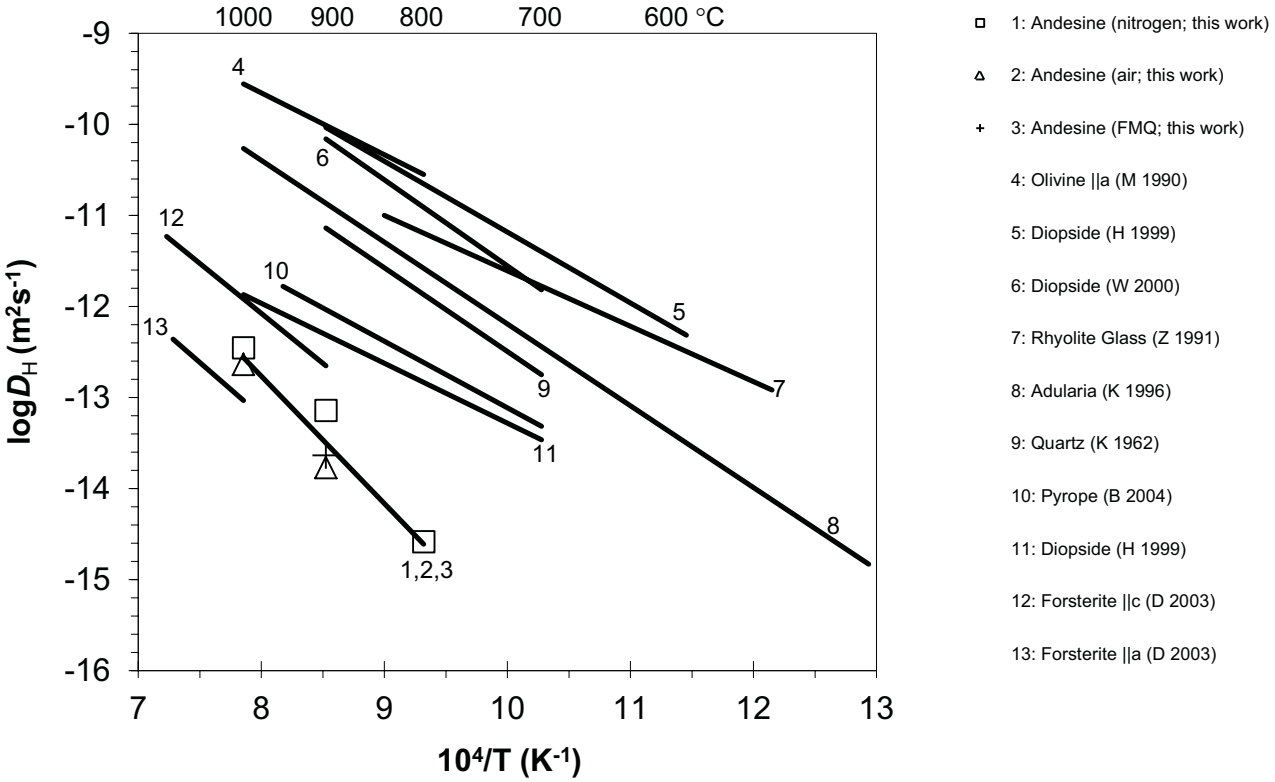
1000
900
800
700
600 °C
-9
-10
-11
-12
-13
-14
-15
-16
7
8
9
10
11
12
13
$\log D_H$ (m^2s^{-1})
$10^4/T$ (K^{-1})
4
6
12
10
13
5
9
7
11
8
1,2,3
1: Andesine (nitrogen; this work)
2: Andesine (air; this work)
3: Andesine (FMQ; this work)
4: Olivine ||a (M 1990)
5: Diopside (H 1999)
6: Diopside (W 2000)
7: Rhyolite Glass (Z 1991)
8: Adularia (K 1996)
9: Quartz (K 1962)
10: Pyrope (B 2004)
11: Diopside (H 1999)
12: Forsterite ||c (D 2003)
13: Forsterite ||a (D 2003)

Figure 6A

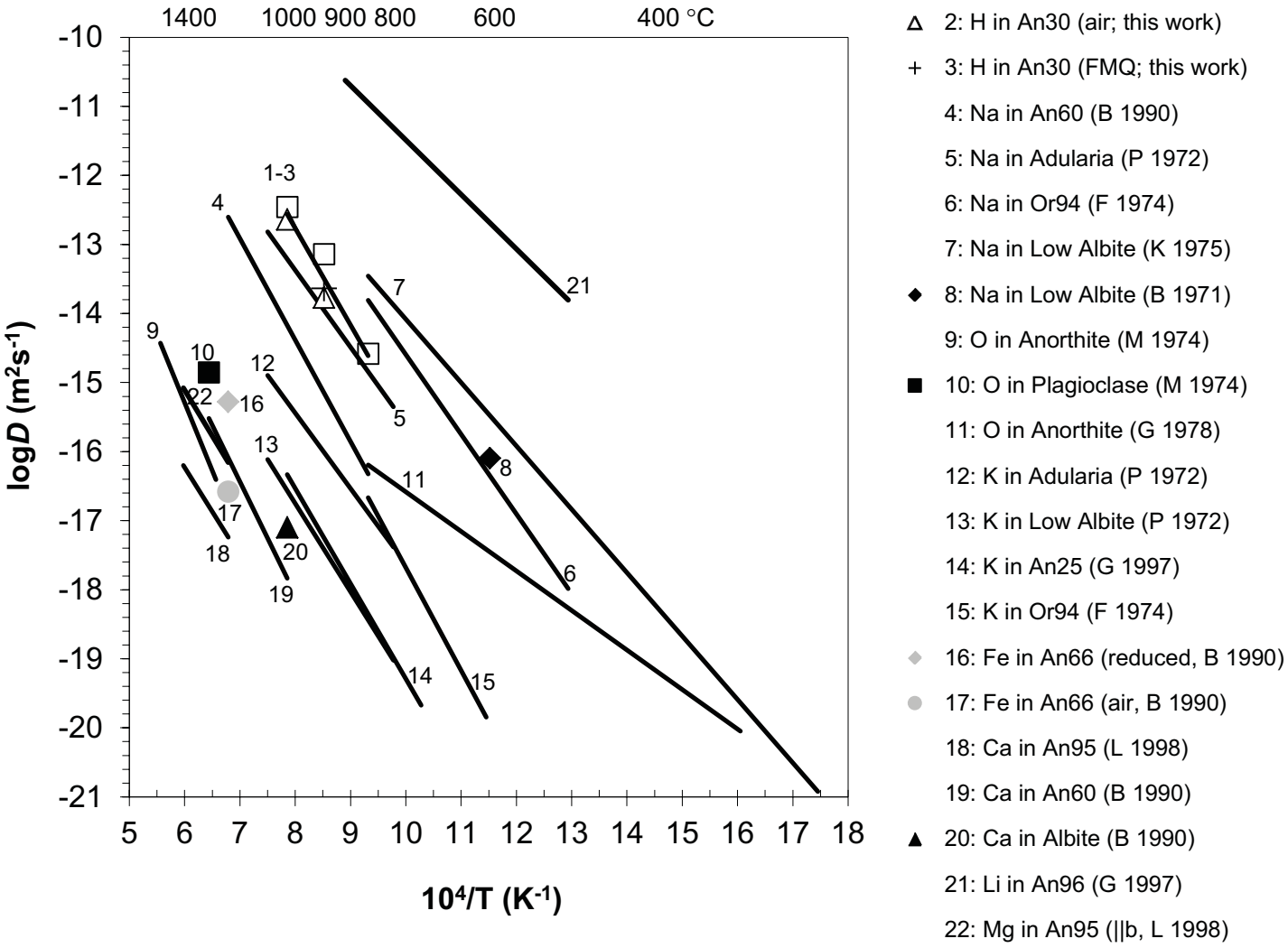
1400
1000 900 800
600
400 °C
-10
-11
-12
-13
-14
-15
-16
-17
-18
-19
-20
-21
log D (m²s⁻¹)
5 6 7 8 9 10 11 12 13 14 15 16 17 18
10⁴/T (K⁻¹)
1-3
4
5
6
7
8
9
10
11
12
13
14
15
16
17
18
19
20
21
22
1: H in An30 (nitrogen; this work)
2: H in An30 (air; this work)
3: H in An30 (FMQ; this work)
4: Na in An60 (B 1990)
5: Na in Adularia (P 1972)
6: Na in Or94 (F 1974)
7: Na in Low Albite (K 1975)
8: Na in Low Albite (B 1971)
9: O in Anorthite (M 1974)
10: O in Plagioclase (M 1974)
11: O in Anorthite (G 1978)
12: K in Adularia (P 1972)
13: K in Low Albite (P 1972)
14: K in An25 (G 1997)
15: K in Or94 (F 1974)
16: Fe in An66 (reduced, B 1990)
17: Fe in An66 (air, B 1990)
18: Ca in An95 (L 1998)
19: Ca in An60 (B 1990)
20: Ca in Albite (B 1990)
21: Li in An96 (G 1997)
22: Mg in An95 (||b, L 1998)

Figure 6B

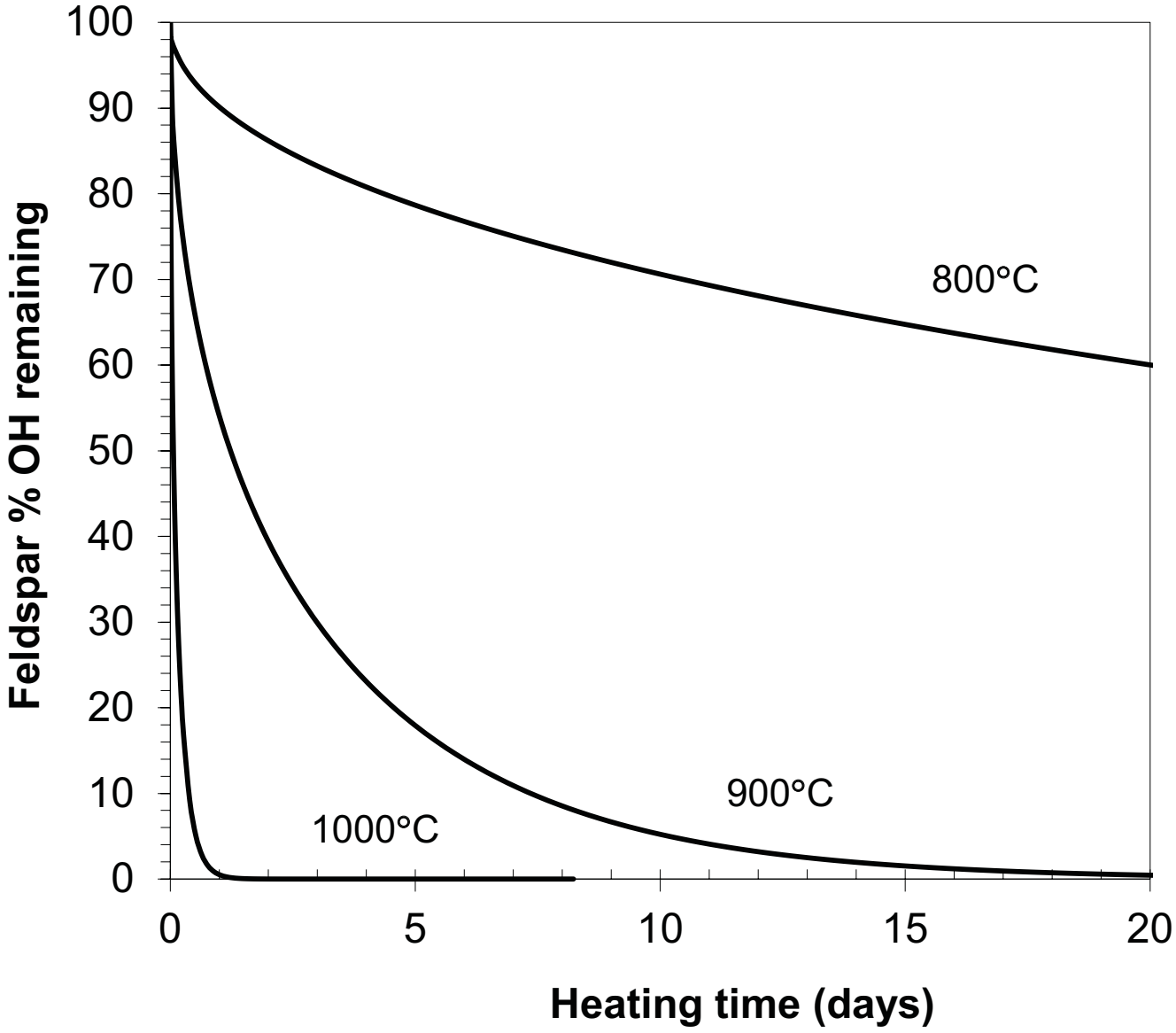
Feldspar % OH remaining
100
90
80
70
60
50
40
30
20
10
0
800°C
900°C
1000°C
0
5
10
15
20
Heating time (days)

Figure 7